Rev. Roum. Sci. Techn.– Électrotechn. et Énerg.
Vol. **71**, *3*, pp. 427–432, Bucarest, 2026

A TRANSFORMERLESS HIGH-GAIN DC-DC CONVERTER FOR ELECTRIC VEHICLE APPLICATIONS

KARTHIKEYAN PALANIYAPPAN[1*], SELVAN PALANIAPPAN [2]

Keywords: Battery energy storage system (BESS); Effective voltage boosting; Electric vehicle (EV); High-gain converter; Renewable energy sources.

Reliable DC power is essential for the continuous operation of battery energy storage systems (BESS) in EV systems. Since these systems require a specific voltage level that many sources cannot directly provide, an efficient voltage-boosting stage is necessary. This paper presents a higher-voltage-gain structure for a non-isolated DC/DC converter with a switched-inductor-based double-switch configuration to step up a low input voltage to a stable high output suitable for EV applications. The proposed converter is analyzed using MATLAB/Simulink to evaluate voltage gain, efficiency, and device stresses. A 100 W hardware prototype producing 200 V output is developed for validation. Both simulation and experimental results confirm improved voltage regulation and reduced output ripple under varying duty conditions. Overall, the topology provides a practical and efficient solution for EV battery energy storage systems.

1. INTRODUCTION

The growing demand for unpolluted energy and sustainable power systems has accelerated the addition of renewable energy sources (RES), for example, solar PV systems, fuel cells, wind energy conversion systems, and energy storage devices. These sources generally produce relatively low DC power that must be boosted to high voltage (HV) levels before they can be effectively utilized in practical applications, such as DC microgrids, electric vehicles (EVs), and hydrogen production systems.

An analog active cell-balancing circuit intended for automotive battery management system (BMS) applications was introduced in [1]. The proposed scheme employed a boost-converter-based balancing method to enhance the operation of series-connected lithium-ion batteries during charging and discharging. Nevertheless, the study primarily emphasized battery balancing functionality and did not focus on step-up gain DC/DC converter design for EV applications. Latreche et al. [2] introduced a synergetic control approach for regulating a DC/DC boost converter system to achieve improved voltage stability and faster transient performance. The developed controller provided better dynamic response under varying load conditions.

Researchers have introduced several advanced power converter configurations that integrate with switched capacitors (SC), switched inductors (SI), and networks with one-switch converter topology proposed in [3], and then a family of integrating active clamp circuit networks (ACCN) and voltage multiplier (VM) for higher-voltage and higher-power applications has been clearly described in [4].

A high-step-up DC/DC converter with a soft-switching configuration was presented in [5] to achieve improved conversion efficiency and continuous input current (CIC) characteristics for renewable energy systems. Subsequently, a reconfigurable high step-up converter with fault-tolerant operation and lower voltage stress was developed in [6] to enhance converter reliability under abnormal conditions. In addition, an ultra-high gain quadratic DC-to-DC converter based on coupled inductors and voltage multiplier cells was introduced in [7] to achieve superior voltage boosting capability.

However, the topologies discussed in [5,7] involve a higher number of passive and magnetic elements, leading to increased converter complexity. A quasi-impedance network (QIN) converter incorporating a voltage spike suppression technique was presented in [8] to provide a higher-boost ratio with lower switch stress and enhanced power converter performance. Similarly, [9,10] presented high-gain step-up converter designs capable of achieving improved voltage-boosting performance while maintaining reduced power-device stress.

Furthermore, comprehensive reviews of HV converter topologies have highlighted the importance of efficient converter design for modern renewable systems. The converters presented in [8–10] employed extra passive and magnetic elements, which leads to increased overall converter complexity. An expandable higher-voltage-gain DC/DC converter with improved efficacy, low voltage stress, and voltage gain was presented in [11]. The works reported in [12,13] mainly investigated boost and multilevel converter configurations for photovoltaic systems to enhance energy extraction capability and power quality. Moreover, a SEPIC-based power-factor-correction topology employing sliding-mode control was developed in [14] for EV charging applications.

Hannan et al. comprehensively reviewed power electronic converter topologies for hydrogen energy systems, emphasizing that high-efficiency DC–DC converters are essential for providing the stable DC voltage required by electrolyzer applications [15]. A mixture zeta-boost converter configuration engaging an active quad switched-inductor configuration was presented in [16] to obtain enhanced voltage gain and better conversion performance. [17] proposed a hybrid transformerless DC–DC converter capable of achieving high voltage gain while minimizing semiconductor voltage stress, making it suitable for high-power conversion applications. [18] developed a single-switch hybrid Boost–Ćuk DC–DC converter that delivers high conversion efficiency and substantial voltage gain with a simple and compact circuit configuration.

A coupled-inductor-based non-isolated super ultra-high step-up dc to dc converter was discussed in [19] to obtain high voltage gain with minimized switch stress. The studies in [20,21] introduced cascade and enhanced high step-up converter structures with leakage energy recovery to improve boosting capability and conversion efficiency. Moreover, bidirectional DC-DC converter configurations for EV applications were discussed in [22,23], respectively.

[1, 2] Department of Electrical and Electronics Engineering, Erode Sengunthar Engineering College, Perundurai, Erode, India.
Emails: pkarthikeyaneee@esec.ac.in (corresponding), hodeee@esec.ac.in

DOI: 10.59277/RRST-EE.2026.3.15

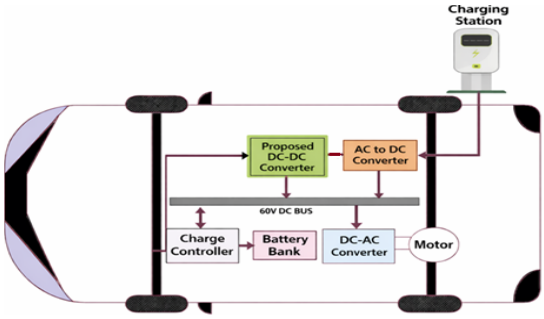

Fig. 1 – Typical application of proposed system.

Difficulties remain in attaining improved efficiency with HV gain while keeping low potential stress across power components and stable operation under varying load conditions. Therefore, further investigation of advanced converter structure is necessary to meet the requirements of battery management system (BMS) and in the automotive industry applications, as demonstrated in Fig. 1. Motivated by these considerations, this studies the design and performance assessment of a high-voltage gain with future of DC/DC converters with non-isolated structures are highly suitable to real-world power conversion answer for HV DC battery energy storage system (BESS) in EV applications for ensuring smooth and reliable operation of BESS.

2. ANALYSIS OF PROPOSED CONVERTER

The configuration of the recommended non-isolated HV power DC-DC converter network is illustrated in Fig. 2.

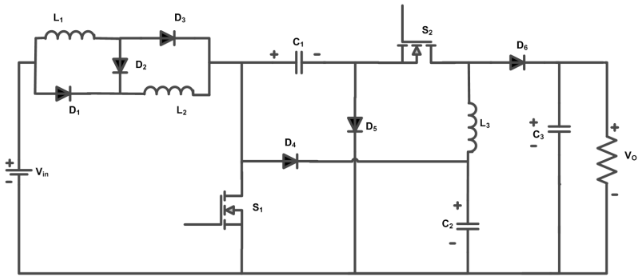

Fig. 2 – Circuit diagram of proposed system.

The proposed network structure consists of two active power electronics switches, S_1 and S_2, three energy storage elements (inductors L_1, L_2, and L_3, three capacitors C_1, C_2, and C_3, and six diodes (D1-D6) to create a current path D_1-D_6. A resistive load R_L is attached to the end of the system. To attain a higher voltage adaptation ratio, a switched-inductor cell is incorporated into the proposed novel circuit topology. The proposed novel HV gain converter is formulated to operate with a minimal duty cycle while still maintaining an HV gain. Both switches are driven simultaneously, which simplifies the control strategy and reduces the complexity of the switching circuitry. The simultaneous switching technique is adopted in the proposed converter to simplify the gating structure and achieve synchronized operation of both MOSFET switches. In real-time implementation, slight switching delays may arise from the propagation delay of the driver and the inherent switching characteristics of the MOSFET. These effects are mainly influenced by the devices' parasitic capacitances, gate charge properties, switching frequency, and manufacturing tolerances. Moreover, the projected converter system operates at a medium switching frequency and employs identical gate drivers with matched MOSFET devices, thereby minimizing delay variation and maintaining stable converter performance. The operation of the HV gain converter is examined through CIC during steady-state conditions. For simplifying the theoretical analysis, all power switching devices, including diodes and switches, are ideal.

The operation of the proposed DC-DC high-boost system can be explained in terms of two distinct operating intervals, namely Mode-I and Mode-II.

2.1 MODES OF OPERATION

The first operating interval corresponds to Mode-I under CIC, as illustrated in Fig. 3 (a). During this interval, both power-electronic controlled switches S_1 and S_2 are ON simultaneously. As a result, diodes D_1 and D_3 become forward-biased, whereas diodes D_2, D_4, D_5, and D_6 remain in a reverse-biased condition. In this state, the input sources supply energy to inductors L_1 and L_2, causing them to store energy. At the same time, inductor L_3 is energized by the capacitors C_1 and C_2. During this interval, the capacitor C_3 discharges its stored energy to the output, thereby maintaining the resistive load current. The equivalent circuitry of this operating condition is shown in Fig. 3 (a).

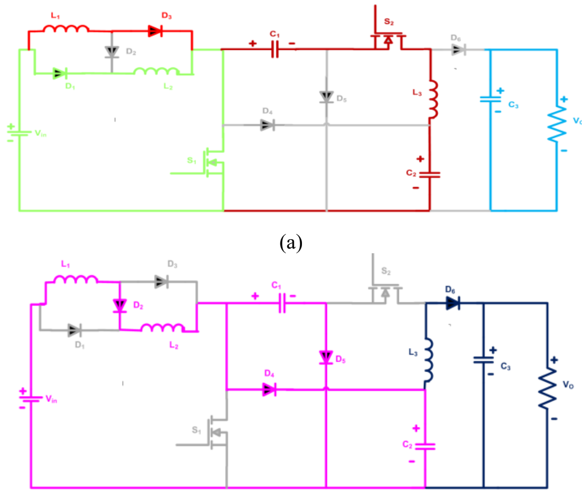

(a)

(b)

Fig. 3 -(a) Mode I and (b) Mode II operation.

The second operating interval, referred to as Mode-II, is illustrated in Fig. 3 (b); both power control switches S_1 and S_2 are in the OFF condition. Consequently, diodes D_2, D_4, D_5, and D_6 become forward-biased, while power diodes D_3 and D_1 remain in a reverse-biased condition. In the course of this stage, the energy kept in inductors L_1 and L_2 is transmitted to capacitors C_1 and C_2 via diodes D_2 and D_4, resulting in their charging condition. Simultaneously, the energy stored in inductor L_3 is distributed to the output capacitor C_3 via power diode D_6. The corresponding circuit representing this operating condition is displayed in Fig. 3 (b). The operating modes confirm that the proposed converter achieves effective energy transfer with enhanced voltage boosting capability for EV applications.

The corresponding mathematical eq. (1)-(3) for Mode-1 and eq. (4)-(6) for Mode- II can be derived using KLV as,

For Mode-1

$$v_{in} = v_{L_1}, \quad (1)$$

$$v_{in} = v_{L_2}, \quad (2)$$

$$-v_{c_1} - v_{c_2} = -v_{L_3}, \tag{3}$$

For Mode-II

$$v_{in} - v_{L_3} = v_{c_3}, \tag{4}$$

$$v_{in} - v_{L_1} - v_{L_2} = v_{c_1}, \tag{5}$$

$$v_{in} - v_{L_1} - v_{L_2} = v_{c_2}. \tag{6}$$

The derived equations eq. (1)-(7) confirm the stable operation with high gain of the proposed system.

2.2 COMPUTATION OF OVERALL VOLTAGE GAIN

The voltage transformation rate of the recommended novel system operating in CIC can be determined based on the volt-second balance principle on inductors L_1 to L_3. By considering the equation derived for Mode-I&II, given in eq. (1)-(6), under steady-state conditions, the voltage gain is expressed as eq. (7) as below,

$$\frac{v_0}{v_{in}} = \frac{(1+D)^2}{(1-D)^2}. \tag{7}$$

2.3 CHIEF OPERATING WAVEFORMS

Figure 4 exemplifies the Chief operating waveforms of the proposed HV gain DC/DC converter system.

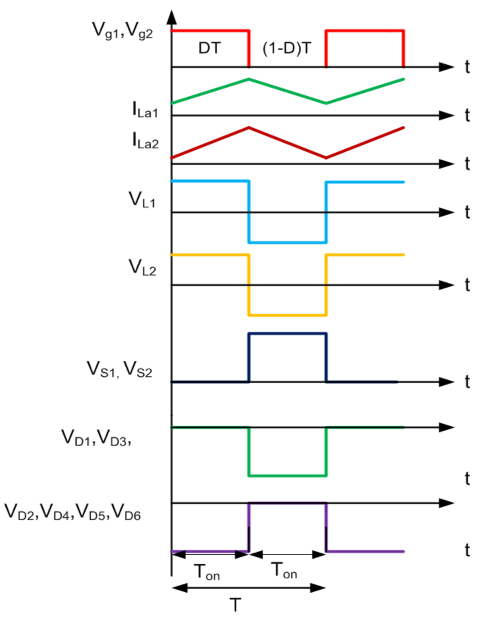

Fig. 4 – Chief operating waveforms.

It ensures the proper charging and discharging behavior of the inductive/capacitive elements, conditional on the gating pulses given to the power switches.

2.4 VOLTAGE AND CURRENT STRESS ACROSS POWER ELECTRONICS DEVICES

The analysis of voltage and current stresses can evaluate the performance of the proposed high-gain converter. The input-side diodes D_1, D_2, and D_3 are subjected to comparatively low voltage stress, whereas the potential stress across diode D_4 is identical to that of power control switch S_1 because of their parallel connection. On the other hand, the output-side diode D_6 experiences high voltage stress, which is nearly half of the load voltage. In terms of current stress, the input-side switches and diodes carry relatively higher current, while the output-side devices mainly conduct the load current. The corresponding stress values of the proposed converter are listed in Table 1.

The derived current/voltage stress equations indicate that the proposed converter maintains acceptable voltage and current stress levels across the power devices.

Table 1

Potential and current stress on power devices of proposed topology.

Components	Potential stress	Current stress
Switch 1,2	$v_{S_1} = v_{in}\frac{(1+D)}{(1-D)}$	$I_{S_1} = \frac{I_{in}}{2}$
	$v_{S_2} = v_{in}\frac{(1+D)^2}{(1-D)^2}$	$I_{S_2} = \frac{(D-1)\,I_{in}}{3D}$
Diodes 1 to 6	$v_{D_1} = v_{D_2} = v_0\frac{(1-D)^2}{(1+D)^2}$	$I_{D_1} = \frac{I_{in}}{2}$
	$v_{D_3} = v_0\frac{(1-D)^2}{(1+D)^2}$	$I_{D2} = I_{in}$
	$v_{D_4} = v_{D_5} = v_{in}\frac{(1+D)}{(1-D)}$	$I_{D_3} = \frac{I_{in}}{2}$
	$v_{D_6} = \frac{3(1+D)}{(1-D)}$	$I_{D_4} = \frac{(2-D)\,I_{in}}{6D-2}$
		$I_{D_5} = \frac{(2-D)\,I_{in}}{6D-2}$
		$I_{D_6} = \frac{(D-1)\,I_{in}}{3D}$

2.5 SELECTION OF COMPONENTS

2.5.1 INDUCTOR DESIGN

Proper inductor selection is important to improve the reliability of the converter and to minimize current ripple, while also decreasing the converter weight and size. During Mode-1, inductors L_1 and L_2 experience the input voltage V_{IN}. Assuming $L_1 = L_2$, the required inductance values are obtained as in eq. (8), where ΔI_L represents the amount of the ripple content of inductors L_1 and L_2, and f_s is the switching frequency of the MOSFET. During Mode-II, inductor L_3 is subjected to the output voltage V_O over the time interval (t). The value of L_3 can be calculated as in eq. (9).

$$L_1 = L_2 = \frac{V_{in}D}{\Delta I_L f_s}, \tag{8}$$

$$L_3 = \frac{2(1+D)V_{in}D}{(1-D)\Delta I_{L_3} f_s}. \tag{9}$$

2.5.2 CAPACITOR DESIGN

The required capacitance values can be designed depending on the acceptable potential ripple content and switching frequency. The elements of capacitors C_1, C_2, and C_3 are calculated from the source current and duty ratio. The design expressions are given in eq. (10)-(12), where ΔV represents the permissible values of potential ripples for capacitors.

$$C_1 = \frac{I_{in}(2-D)D}{(6D-2)D\Delta V_1 f_s}, \tag{10}$$

$$C_2 = \frac{I_{in}(2-D)D}{(6D-2)D\Delta V_{C_2} f_s}, \tag{11}$$

$$C_3 = \frac{I_0 D}{D\Delta V_{C_3} f_s}. \tag{12}$$

The obtained inductor and capacitor values confirm the fitness of the proposed system with small ripples.

3. DISCUSSIONS ON SIMULATION OUTPUTS AND HARDWARE RESULTS

A MOSFET operating frequency of 20 kHz was designated to provide a suitable trade-off between efficiency and converter size. Operating at lower frequencies requires large passive components, whereas higher frequencies increase semiconductor stress and heating. Therefore, 20 kHz offers satisfactory converter performance with manageable efficiency, stress, and compact component design. The performance of the high-gain novel converter is evaluated through simulations carried out in MATLAB. To confirm the simulation outcomes, a hardware setup model of the system is also developed and confirmed. The values of parameter settings used during the simulation study are provided in Table 2.

Table 2

System parameter values used in simulation

Parameters	Values
V_{in}	20V
$L_{1,2}$	0.5 mH
L_3	1.5 mH
C_1	470 µF
C_2	470 µF
C_3	100 µF
V_o	200 V
P_{out}	100 W
fs	20 kHz
R_L	400 Ω

3.1 SIMULATION OUTCOMES UNDER CLOSED LOOP CONDITION

To maintain a stable output voltage level of 200V under different operating condition, during a PI controller is employed in the simulation. Figure 5 shows the desirable output voltage waveform of the proposed novel HV gain converter working under closed-loop control. The converter attains the desired output voltage level of 200V at a rated resistive load value of 400 Ω within approximately 0.3 s, while maintaining very minimal voltage ripple**.**

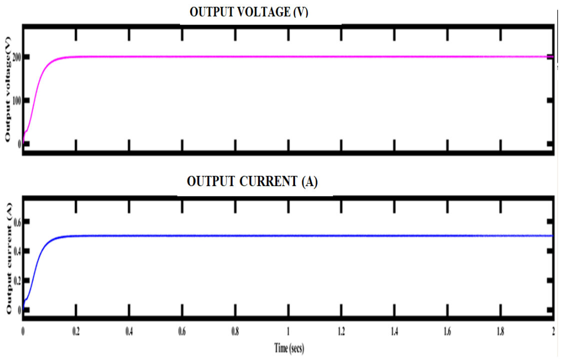

Fig. 5 – Output waveform under closed-loop condition.

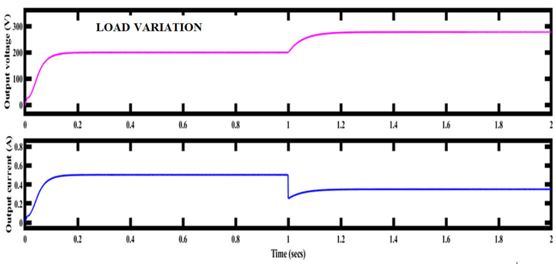

Fig. 6 –Performance of the proposed converter under load variation.

To evaluate the dynamic behavior of the proposed converter, sudden changes in load conditions were introduced during the simulation analysis. The assessment of the DC/DC converter system was examined through output voltage and output characteristics, as demonstrated in Fig. 6. Initially, the converter operated with a 400 Ω resistive load, and at t = 1 s, the load resistance was changed to 800 Ω, representing a 200% variation from the initial load condition. Following this transition, the load voltage increased to nearly 283 V, while the output current gradually decreased and settled at approximately 0.35 A. These results demonstrate that the converter maintains stable operation and satisfactory regulation performance under varying load conditions

3.2 HARDWARE RESULTS AND DISCUSSIONS

The hardware prototype was realized using a regulated DC power supply (RPS), digital storage oscilloscope (DSO), and measure the voltage across the resistive load, capacitors, diodes and then switches using voltage sensing probes. Similarly, inductor current was measured using a current-sense probe, and a MOSFET gate-driver circuitry was used to generate the gating pulse for the power switch; a digital multimeter was used to measure the voltage across each power component. All experiment measurements and waveform analyses were performed under steady-state conditions. The proposed converter was verified with a source voltage of 20 V to obtain a load voltage of 200 V at a MOSFET operating frequency of 20 kHz and a duty cycle of 52%. The prototype employed L_1 and L_2 inductors of 0.5 mH, L_3 of 1.5 mH, C_1 and C_2 capacitors of 470 µF, and C_3 of 100 µF. Experimental validation was carried out at a rated output power of 100 W with a 400 Ω load resistance. In addition, the output voltage characteristics were observed under open-loop conditions. The voltage and current signals were captured using calibrated probes interfaced with the oscilloscope to ensure reliable evaluation of the converter performance.

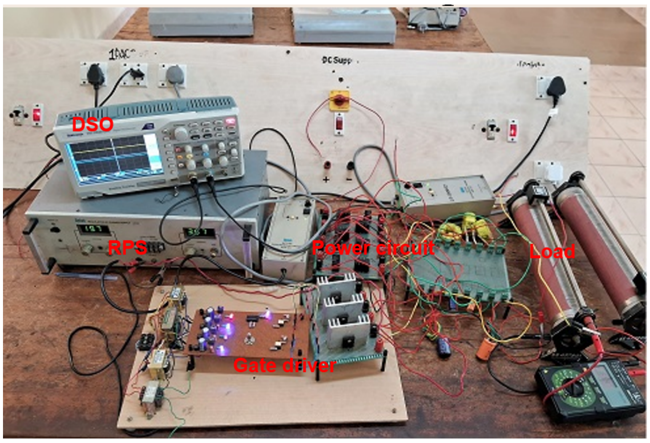

Fig. 7 – Hardware step-up.

The load current of the new converter is 0.5 A. The hardware provisions of the proposed converter are listed in Table 3.

Table 3

Hardware specifications of the proposed converter

Component	Rating
Fast Recovery diode	6A10 (1000 V & 10 A)
Switch MOSFET	IRF540N (100 V & 33 A)
Inductor	0.5 mH, 0.5 mH, 1.5 mH
Capacitor	1000 µF, 1000 µF, 2200 µF

Figure 8 presents the gating signal along with the matching output voltage waveform. The current in the inductors L_1, L_2, and L_3 is illustrated in Figs. 9, 10, and 11, respectively. The potential levels on the power control switches and diodes are shown in Figs. 12 to19. These figures indicate that the potential stress is on diodes D_1 to D_6.

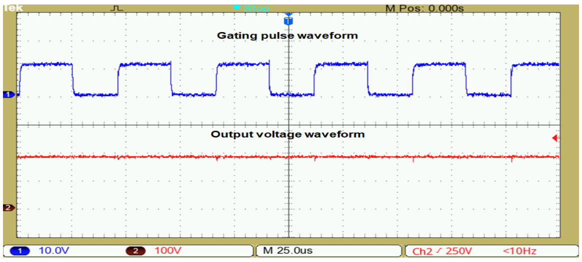

Fig. 8 –Output voltage.

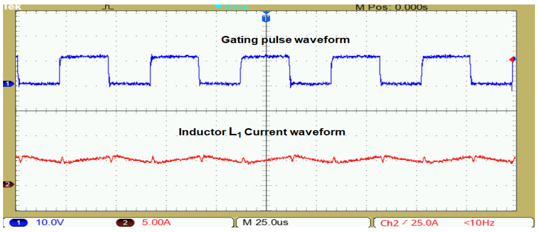

Fig. 9 – Current flow through inductor L_1.

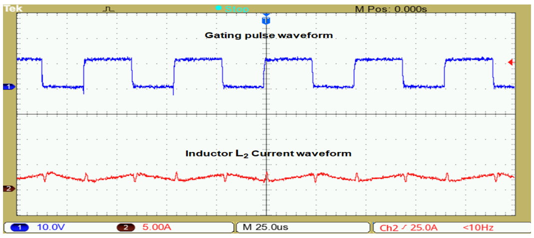

Fig. 10 –Current flow through inductor L_2.

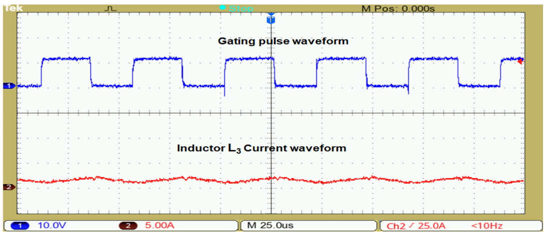

Fig. 11 – Current flow through inductor L_3.

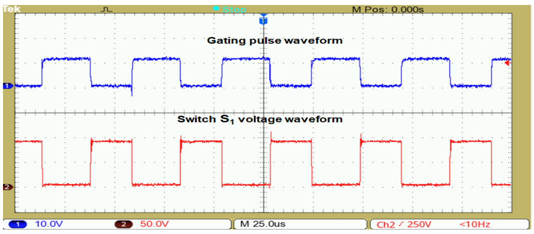

Fig. 12 –Voltage across switch S_1.

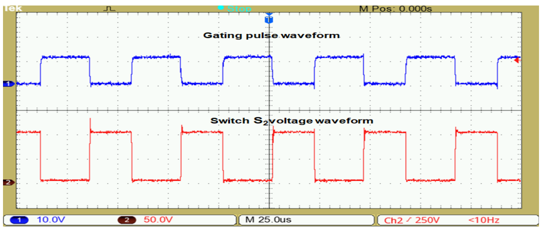

Fig. 13 – Voltage across switch S_2.

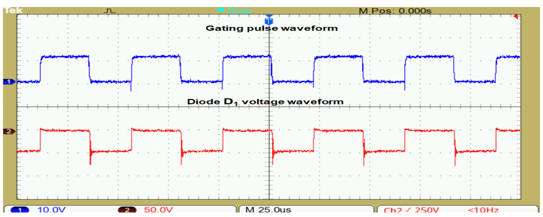

Fig. 14 –Voltage across Diode D_1.

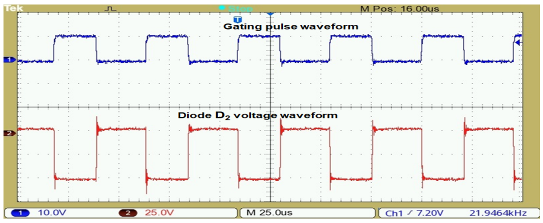

Fig. 15 –Voltage across Diode D_2.

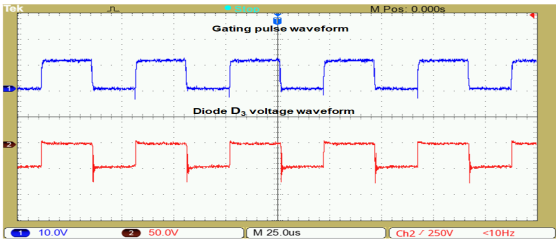

Fig. 16 –Voltage across Diode D_3.

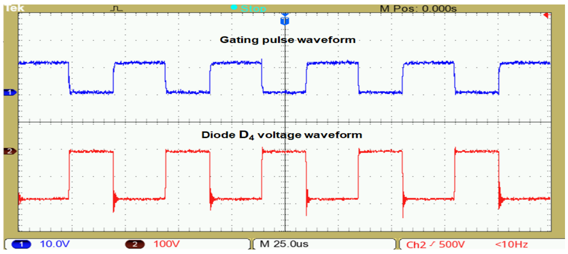

Fig. 17 –Voltage across Diode D_4.

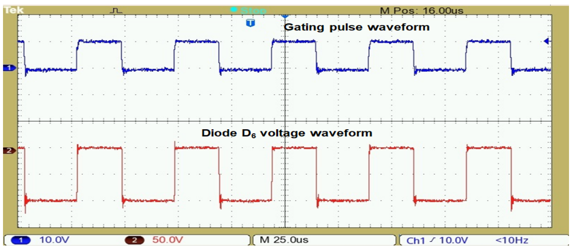

Fig. 18 –Voltage across Diode D_5.

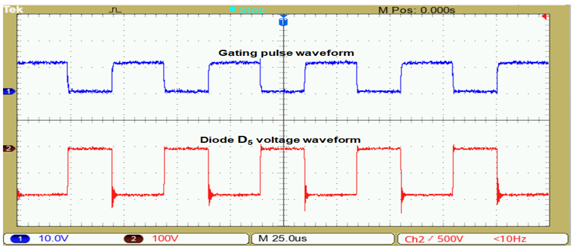

Fig. 19 –Voltage across Diode D_6.

4. CONCLUSIONS

A transformer-less quadratic DC/DC high gain converter intended for BESS application in this work. The proposed topology utilizes switched inductor and capacitor configurations to attain a higher output voltage adaptation ratio while maintaining a simple circuitry structure. The operating principles and performance characteristics of the converter were investigated through both simulation and hardware implementation. The proposed converter was operated with a 20 V input supply and generated an output voltage of 200 V and an output power of 100 W at a duty cycle of 52%. To examine the dynamic response, the converter was tested with varying load conditions by changing the resistive load from 400 Ω to 800 Ω. Under this condition, the load voltage amplified to nearly 283 V, whereas the output current reduced and settled around 0.35 A, indicating satisfactory regulation and stable converter operation. The proposed system operated at a MOSFET operating frequency of 20 kHz, which offered a balanced compromise between converter efficiency and passive component size. In addition, simultaneous switching operation simplified the control circuit and reduced switching control complexity. The experimental observations were found to match the simulation outcomes, confirming the soundness and reliability of the converter design. Despite the advantage of ultra-voltage gain and reduced structural complexity, certain practical limitations were observed, including increased voltage stress across semiconductor devices and switching losses during high-frequency operation. Therefore, further research can be directed toward improving efficiency, minimizing device stress, and enhancing converter performance for higher power applications. Overall, the proposed converter topology provides an effective solution for battery energy storage systems requiring high step-up voltage conversion and stable operating performance in EV applications for the automotive industry.

Future work can focus on extending the new converter to ultra-high power for automotive applications. Advanced control techniques can be introduced to improve voltage regulation and dynamic response. Further investigation into thermal performance will help evaluate its suitability for continuous operation. In addition, reducing component size and improving power density can make the converter more compact and economical.

ACKNOWLEDGEMENTS

The authors wish to express their sincere gratitude to the management and the principal of Erode Sengunthar Engineering College (Autonomous), Perundurai, Erode, Tamil Nadu, India, for their valuable support and for providing the required research facilities to undertake this work in collaboration with Anna University, Chennai, and Tamil Nadu. India.

CREDIT AUTHORSHIP CONTRIBUTION STATEMENT

KARTHIKEYAN PALANIYAPPAN: main conceptual ideas, design, simulation, hardware, and manuscript preparation.

SELVAN PALANIAPPAN: supervision, validation, review, and proofreading.

Received on 19 March 2026

REFERENCES

1. B. Anton, A. Florescu, S.G. Rosu, "Standalone analog active cell-balancing circuit for automotive battery management systems." Revue Roumaine Science Techniques – Électrotechnique et Énergétique, **63**, *3*, pp. 306–313 (2018).
2. S. Latreche, B. Babes, A. Bouafassa, "Design and real-time implementation of synergetic regulator for a DC-DC boost converter", Rev. Roum. Sci. Techn. – Électrotechn. et Énerg., **69**, *3*, pp. 305–310 (2024).
3. R.A. Khan, H.-D. Liu, C.-H. Lin, S.-D. Lu, S.-J. Yang, A. Sarwar, "A novel high-voltage-gain step-up DC–DC converter with maximum power point tracker for solar photovoltaic systems." Processes, **11**, pp. 1–17 (2023).
4. R. Beiranvand, S.H. Sangani, "A family of interleaved high step-up DC–DC converters integrating voltage multiplier and active clamp circuits." IEEE Access, **11**, pp. 1–15 (2023).
5. H.M. Jazi, R.R. Khorasani, E. Adib, P. Zanchetta, G. Velasco-Quesada, H. Martínez-García, "A high-efficient single-switch soft-switching high step-up DC–DC converter with continuous input current for renewable energy integration." IEEE Transactions on Power Electronics, **39**, pp. 9814–9825 (2024).
6. K. Velmajala, S.R. Sandepudi, "High step-up DC–DC converter with reconfiguration capability." IEEE Latin America Transactions, **22**, pp. 971–982 (2024).
7. S.P. Sharma, S. Hasanpour, R. Kumar, "Ultra-high voltage gain achieved with quadratic DC/DC converter design", Scientific Reports, **14**, 23384 (2024).
8. H. Sridharan, S. Ramalingam, J. Arumugam, "Wide boost ratio in quasi-impedance network converter using switch voltage spike reduction technique", Rev. Roum. Sci. Techn. – Électrotechn. et Énerg., **68**, *3*, pp. 259–265 (2023).
9. R. Rostami, S.H. Hosseini, M.B.B. Sharifian, "High-gain non-isolated step-up DC–DC converter suitable for renewable energy applications." Scientific Reports, **15**, pp. 1–14 (2025).
10. S. Mohsen Salehi, A.Y. Varjani, "A step-up DC-DC converter with high voltage gain and soft-switched capability and minimum phase characteristic", Scientific Reports, **16**, 9763 (2026).
11. M.B. Patel, J. Nakka, P.K. Bonthagorla, "Design and analysis of a very high-gain expandable DC–DC step-up converter." IEEE Access, **14**, pp. 1–15 (2026).
12. S. Seba, M. Birane, K. Benmouiza, "A comparative analysis of boost converter topologies for photovoltaic systems using maximum power point (P&O) and beta methods under partial shading." Rev. Roum. Sci. Techn. – Électrotechn. et Énerg., **68**, *4*, pp. 375–380 (2023).
13. M.-A. Ilie, D. Floricău, "Grid-connected photovoltaic systems with multilevel converters – modeling and analysis." Rev. Roum. Sci. Techn. – Électrotechn. et Énerg., **68**, *1*, pp. 77–83 (2023).
14. D. Ziane, A. Azib, A. Oubelaid, N. Taib, T. Rekioua, D. Rekioua, "Proposed power factor correction circuit based on the single-ended primary-inductor converter controlled by sliding mode control strategy used in an electric vehicle charging station." Rev. Roum. Sci. Techn. – Électrotechn. et Énerg., **67**, *3*, pp. 241–245 (2022).
15. P. Pilati, R. Mandrioli, V. Cirimele, M. Ricco, D. Guillbert, "Power electronic converters for green hydrogen production from photovoltaic: A review", International Journal of Hydrogen Energy, **270**, 157013 (2026).
16. M.S. Bhaskar, N. Gupta, S. Selvam, D.J. Almakhles, P. Sanjeevikumar, J.S.M. Ali, S. Umashankar, "A new hybrid Zeta-boost converter with active quad switched inductor for high voltage gain." IEEE Access, **9**, pp. 20022–20034 (2021).
17. A.M.S.S. Andrade, T.M.K. Faistel, R.A. Guisso, A. Toebe, "Hybrid high voltage gain transformerless DC–DC converter." IEEE Transactions on Industrial Electronics, **69**, *3*, pp. 2470–2479 (2022).
18. A.M.S.S. Andrade, T.M.K. Faistel, R.A. Guisso, "Single-switch high-efficiency hybrid boost–Ćuk DC/DC converter with high-voltage gain and low-voltage stress." IET Power Electronics, **13**, *12*, pp. 2538–2546 (2020).
19. A. Nadermohammadi, M. Maalandish, A. Seifi, P. Abolhassani, S.H. Hosseini, M. Farsadi, "A non-isolated single-switch ultra-high step-up DC–DC converter with coupled inductor and low-voltage stress on switch", IET Power Electronics, **17**, pp. 251–265 (2024).
20. J. Ai, M. Lin, M. Yin, "A family of high step-up cascade DC–DC converters with clamped circuits." IEEE Transactions on Power Electronics, **35**, *5*, pp. 4819–4834 (2020).
21. H. Chen, X. Hu, Y. Huang, M. Zhang, B. Gao, "Improved DC–DC converter topology for high step-up applications." IET Circuits, Devices & Systems, **13**, *1*, pp. 51–60 (2019).
22. T.-I. Voicila, G.-C. Seritan, B.-A. Enache, "Analysis of bidirectional DC–DC power converters for screening systems of retired batteries." Rev. Roum. Sci. Techn. – Électrotechn. et Énerg., **69**, *3*, pp. 311–316 (2024).
23. G. Jothimani, K. Mahalingam, P. Karuppasamy, "A double-switch integrated high-gain quadratic boost converter for electric vehicle applications." Rev. Roum. Sci. Techn. – Électrotechn. et Énerg., **70**, *4*, pp. 495–500 (2025).